ACS APPLIED MATERIALS & INTERFACES

Research Article

www.acsami.org

Contactless Photoconductance Study on Undoped and Doped Nanocrystalline Diamond Films

Venkatesh Seshan,[†,‡,#] Dharmapura H. K. Murthy,[†,⊥,#] Andres Castellanos-Gomez,[‡] Sumit Sachdeva,[†] Hakeem A. Ahmad,[†] Stoffel D. Janssens,[§,∥] Wiebke Janssen,[§,∥] Ken Haenen,[§,∥] Herre S. J. van der Zant,[‡] Ernst J. R. Sudhölter,[†] Tom J. Savenije,[*,†] and Louis C. P. M. de Smet[*,†]

[†]Department of Chemical Engineering, Delft University of Technology, Julianalaan 136, 2628 BL Delft, The Netherlands

[‡]Kavli Institute of Nanoscience, Delft University of Technology, Lorentzweg 1, 2628 CJ Delft, The Netherlands

[⊥]Dutch Polymer Institute (DPI), 5600 AX Eindhoven, The Netherlands

[§]Institute for Materials Research (IMO), Hasselt University, Wetenschapspark 1, BE 3590 Diepenbeek, Belgium

[∥]IMOMEC, IMEC vzw, Wetenschapspark 1, BE 3590 Diepenbeek, Belgium

ABSTRACT: Hydrogen and oxygen surface-terminated nanocrystalline diamond (NCD) films are studied by the contactless time-resolved microwave conductivity (TRMC) technique and X-ray photoelectron spectroscopy (XPS). The optoelectronic properties of undoped NCD films are strongly affected by the type of surface termination. Upon changing the surface termination from oxygen to hydrogen, the TRMC signal rises dramatically. For an estimated quantum yield of 1 for sub-bandgap optical excitation the hole mobility of the hydrogen-terminated undoped NCD was found to be ~0.27 $cm^2/(V\ s)$ with a lifetime exceeding 1 μs. Assuming a similar mobility for the oxygen-terminated undoped NCD a lifetime of ~100 ps was derived. Analysis of the valence band spectra obtained by XPS suggests that upon oxidation of undoped NCD the surface Fermi level shifts (toward an increased work function). This shift originates from the size and direction of the electronic dipole moment of the surface atoms, and leads to different types of band bending at the diamond/air interface in the presence of a water film. In the case of boron-doped NCD no shift of the work function is observed, which can be rationalized by pinning of the Fermi level. This is confirmed by TRMC results of boron-doped NCD, which show no dependency on the surface termination. We suggest that photoexcited electrons in boron-doped NCD occupy nonionized boron dopants, leaving relatively long-lived mobile holes in the valence band.

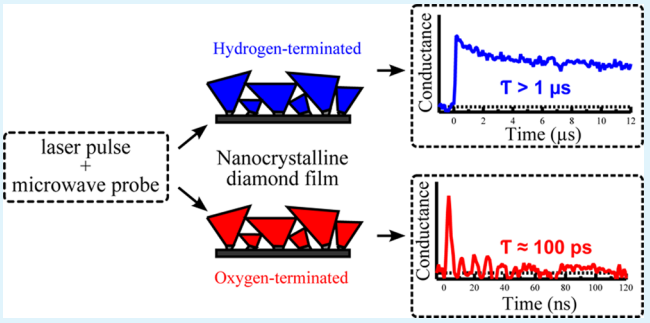

KEYWORDS: *photoconductance, nanocrystalline diamond, TRMC, carrier lifetime, mobility, contactless*

I. INTRODUCTION

Since the past decade, the interest in diamond research, especially in nanocrystalline diamond (NCD) films, has grown significantly because of its unique material properties. NCD films exhibit high chemical stability in harsh environments, allow biochemical surface functionalization, and can be doped with impurities to alter its electronic properties.[1,2] Furthermore, NCD films can be fabricated on wafer-scale at low-cost using the chemical vapor deposition (CVD) technique. As a result, NCD films could be a solution to the growing need for an alternate electrode material in photovoltaic applications.[3,4]

NCD films are made of crystalline diamond grains that are surrounded by nondiamond residual material such as sp^2 carbon phases and carbon with distorted sp^3 bonds and dangling bonds at the grain boundaries.[5−7] Even though the diamond grains dominate the composition of the NCD films, the presence of defect states in the bulk of the material and also, defect states at the diamond surfaces affect the optoelectronic properties of the films.[6−9] As a consequence, there is an increasing demand for a better understanding of the factors affecting the optoelectronic properties to further control and improve the film quality. Several studies on the defect distribution in the microcrystalline and NCD films using photocurrent measurements have been reported.[10−13] In addition, the influence of experimental conditions such as ambient temperature, ultraviolet light irradiation, and air pressure on photoexcited charge characteristics using photoluminescence techniques have also been discussed.[14−16] Although photoluminescence techniques give important information on charge carrier dynamics of sub-bandgap states in NCD films, it is found to be less sensitive to the surface termination effect.[17] Additionally, the surface properties of NCD films are significantly affected by hydrogen and oxygen termination in terms of surface wettability, electrical con-

Received: March 31, 2014
Accepted: June 11, 2014
Published: June 11, 2014

ductivity and electron affinity.[18,19] Therefore, it is imperative to study the effect of surface termination on the charge carrier kinetics and degree of Fermi level pinning using a complementary technique that can investigate surface sensitivity for better understanding of the fundamental charge generation and recombination processes in NCD films.

In the current article, the influence of the type of surface termination and boron and phosphorus doping, on the photoconductive properties of NCD films using the contactless time-resolved microwave conductivity (TRMC) technique are presented and discussed in detail. One very important characteristic of the TRMC technique is that no electrical contacts to the film are needed. As a result this approach overcomes contact problems that can be present in conventional photoconductivity measurements, including non-Ohmic contacts, contact resistance and adhesion problems. In addition to TRMC, valence band spectra of the NCD films are studied using X-ray photoelectron spectroscopy (XPS).

2. EXPERIMENTAL SECTION

Hereafter, we will refer to undoped NCD, boron-doped NCD and phosphorus-doped NCD films as undoped NCD, B-NCD and P-NCD, respectively. All the NCD (undoped and doped) films were grown on quartz substrates under similar conditions. Prior to the CVD growth, the quartz substrates were seeded with diamond nanoparticles with a diameter of 7−10 nm.[20] The deposition of the NCD films was carried out using microwave plasma-enhanced CVD using standard H_2/CH_4 plasma. The reactor conditions for the film growth can be found in this work.[21] The CVD deposition was stopped when the thickness reached ∼150 nm based on the in situ laser interferometer reading, which was followed by cooling down the films in the presence of a H_2 flow. This procedure yielded an undoped NCD film with hydrogen termination (undoped NCD:H) on the surface. For the growth of B-NCD and P-NCD films, trimethylboron (boron concentration ∼3000 ppm) and phosphine (phosphorus concentration ∼10 000 ppm) gases were introduced, respectively, during the CVD process.

For photochemical oxidation, the as-grown NCD:H (undoped and doped) films were exposed to ultraviolet (UV) light under ambient conditions for ∼4 h using a UV/Ozone ProCleaner system (BioForce Nanosciences Inc.). This treatment resulted in NCD films with oxygen termination (NCD:O). Oxidized NCD films were rehydrogenated using a nonplasma quartz tube reactor at ∼850 °C for 20 min in the presence of H_2 gas, followed by gradual cooling to room temperature under a continuous H_2 flow to obtain NCD:H films. The details of hydrogen termination using H_2 gas can be found in this work.[22] The cycle of reoxidation and rehydrogenation of NCD films was repeated at least 2 times to cross verify the characterization results obtained from the changes in film properties due to the change in surface termination. The hydrogenated and oxygenated NCD films were stored in air at room temperature.

The following part describes different characterization techniques performed on undoped and doped NCD films. The surface wettability of hydrogenated and oxygenated NCD films was studied using an Easy Drop goniometer (Krüss GmbH, Germany). A drop of 1 μL of Milli-Q water was dispensed on the NCD film to examine the static water contact angle using drop-shape analysis software. To obtain an average water contact angle (WCA), we performed measurements at more than 5 different spots on the film.

To estimate the average (surface) grain size and the surface roughness of the NCD films, we performed tapping-mode atomic force microscopy (AFM) with a Nanoscope Dimension 3100 scanning probe microscope using silicon cantilevers (OLYMPUS) with a resonance frequency of ∼350 kHz and a spring constant of ∼26 N/m.

Raman spectroscopy was performed at 514 nm excitation wavelength with a laser spot size of ∼400 nm using a Renishaw in via micro-Raman spectrometer to identify the sp^3 bonding characteristics, i.e., the diamond phase of the NCD film.

The valence band measurements of NCD films were carried out using a monochromated Al K_α XPS (Thermo Fisher Scientific, K Alpha model). XPS measurements were performed at a base pressure of 10^{-7} mbar with a spot size of 400 μm. Valence band scans were taken at 100 eV pass energy at 3 different spots on the film with each scan averaged over 10 times. The flood gun was kept on during all XPS measurements to compensate for the potential charging of surfaces.

Optical transmission (I_T) and reflection (I_R) spectra of the NCD films were measured using a PERKIN ELMER Lambda 900 UV/vis/NIR spectrometer. The spectra were used to obtain the fraction of incident photons absorbed (F_A) by the film, which is given by

$$F_A = 1 - (I_T + I_R)/I_0 \quad (1)$$

where I_0 is the incident light intensity.

Photoconductance measurements on the NCD films were carried out using the TRMC technique at room temperature and ambient pressure. Previously, this technique has been used to study the charge transport properties in a wide range of materials including organic blend films and (nanostructured) inorganic semiconductors.[23−25] In one of our recent studies, we used the TRMC technique for the first time to study diamond films in an electrode-free way.[22] A new method to hydrogenate CVD diamond films by high-temperature annealing at atmospheric pressure was introduced. To compare the resulting films with films that were hydrogenated with the established plasma-based method, we used a variety of techniques, including TRMC. A detailed description on the TRMC technique can be found in this review.[25] Briefly, the home-built TRMC setup consists of an X-band (8.4 GHz) microwave cell (Figure 1). The NCD film was photoexcited with a 3

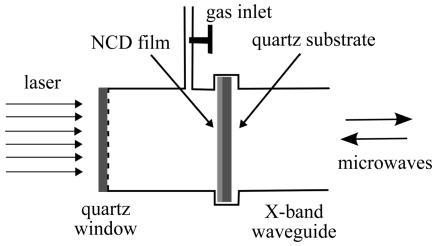

Figure 1. Schematic of the microwave cell used in the TRMC technique.

ns laser pulse from an optical parametric oscillator pumped by a Q-switched Nd:YAG laser (Vibrant II, Opotek). The overall response time of the setup including the electronics used for detection is ∼1 ns. The measurements were performed at 300 nm (4.13 eV), 580 nm (2.14 eV), and 700 nm (1.77 eV) wavelengths, which all correspond to energies smaller than the bandgap of diamond.

Photoexcitation of the NCD film results in the generation of mobile charge carriers in the film, which consequently changes the conductance (ΔG) of the film. Because there is no external electrode/contact to the film, the photogenerated mobile charges eventually decay with time via recombination and/or trapping. The change in conductance within the film ($\Delta G(t)$) can be related to the normalized change in the reflected power ($\Delta P(t)/P$) from the microwave cell and is given by[25]

$$\Delta P(t)/P = -K\Delta G(t) \quad (2)$$

where K represents a sensitivity factor that is determined from the dimensions of the microwave cell and the geometrical properties of the media in the microwave cell. The time-dependent change in conductance ($\Delta G(t)$) can be further expressed in terms of the number of photoinduced electrons and holes and the sum of their mobilities. If the decay of the photoinduced charges is longer than the time resolution of the detection system, then the maximum change in conductance (ΔG_{max}) with respect to the incident light gives the following equation

$$\Phi\Sigma\mu = \Delta G_{max}/\beta e I_0 F_A \quad (3)$$

Here, $\Phi\Sigma\mu$ denotes the product of the quantum yield of the photoinduced charges (Φ) per absorbed photon and the sum of electrons and holes mobilities ($\Sigma\mu$), I_0 is the incident light intensity per pulse, and F_A is the fraction of incident photon absorbed. β is the ratio between the broad and narrow internal dimensions of the microwave cell and e is the electron charge.

3. RESULTS AND DISCUSSION

In the first part of this section, we elaborate on the film characterization, which includes WCA for surface wettability, AFM for surface topography and grain size, Raman spectroscopy for the presence of crystalline diamond phase, and XPS measurements for valence band profile. The second part focuses on the TRMC photoconductance data of hydrogen and oxygen-terminated NCD; undoped, boron-doped, and phosphorus-doped.

To evaluate the surface wetting properties, we carried out WCA measurements. For boron-doped, phosphorus-doped and undoped NCD:O films, the average static water contact angle was found to be less than 20°, whereas values of 80−90° were found for the corresponding NCD:H films, which is in line with reported values.[26]

For characterizing the topography and the surface grain size of the NCD surface, we performed AFM. Figure 2 depicts AFM topography images of undoped NCD:O, B-NCD:O and P-NCD:O films showing the nanocrystalline character of the films with a high density of grains. The average surface grain sizes of the undoped NCD:O, B-NCD:O and P-NCD:O films were found to be ∼60, ∼128, and ∼78 nm, respectively, and the root-mean-square values of the surface roughness were found to be ∼17, ∼29, and ∼47 nm, respectively.

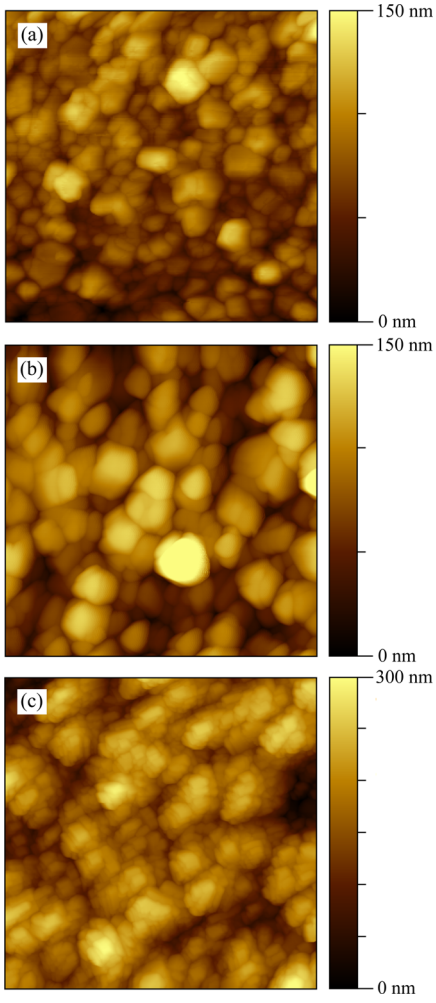

Figure 2. AFM topography images (2 μm × 2 μm) of (a) undoped NCD:O, (b) B-NCD:O, and (c) P-NCD:O films.

To identify the sp^3 phase in the NCD films, we carried out Raman spectroscopy. Figure 3 presents the Raman spectra of hydrogen- and oxygen-terminated undoped NCD, B-NCD and P-NCD films with a peak (ii) at 1329, 1321, and 1330 cm^{-1}, respectively, which corresponds to the sp^3 vibrational mode of diamond.[27,28] The broadening and shifting of the diamond peak from the characteristic 1332 cm^{-1} line can be associated with the grain size of the NCD film and the eventual presence of strain.[27] The peaks observed at 1135 and 1475 cm^{-1} for undoped NCD and peaks 1150 and 1477 cm^{-1} for B-NCD (i.e., peaks i and iii in both cases) correspond to the C−H vibration modes, which also have been reported previously in these kind of films.[29] The broad hump around 1550 cm^{-1} for undoped NCD (peak iv), 1600 cm^{-1} for B-NCD (peak iv) and 1550 cm^{-1} for P-NCD (peak i) are attributed to sp^2-bonded carbon, which is predominantly expected to be present at the grain boundaries.[30,31] Finally, the peak observed at 1220 cm^{-1} for B-NCD film (peak v) can be ascribed to boron doping.[32,33]

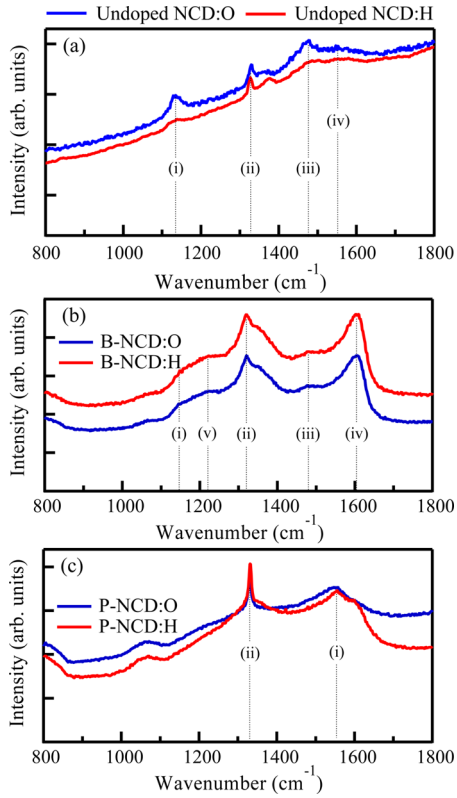

Figure 3. Raman spectra of (a) undoped NCD, (b) B-NCD, and (c) P-NCD films.

To further characterize the surface of NCD films, we carried out XPS valence band measurements. Figure 4 shows XPS valence band spectra for undoped and doped NCD films. The undoped NCD:H plot consists of 4 features as identified by ref 34 (Figure 4a, dashed lines): (i) a peak below ∼11 eV is attributed to the valence bands related to the C 2p levels, which

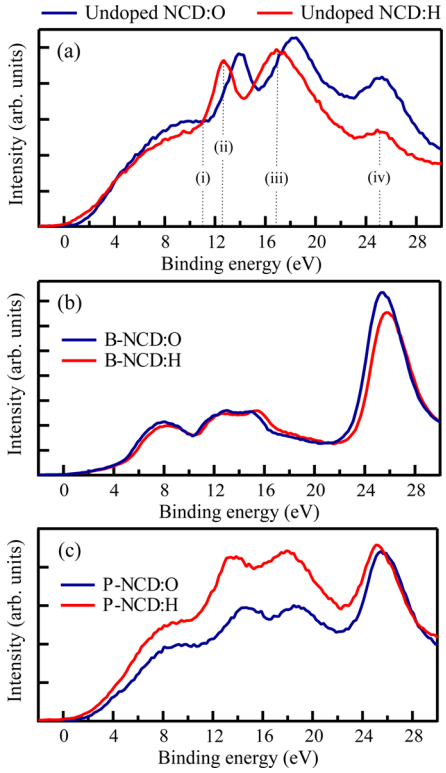

Figure 4. XPS valence band spectra of (a) undoped NCD, (b) B-NCD, and (c) P-NCD films.

are linked to H 1s orbitals, (ii) a peak around ~12 eV that corresponds to the valence band derived from the 2s−2p hybridized levels of the diamond, (iii) a peak around ~17 eV related to the 2s level of the diamond and (iv) a low-intensity peak around ~25 eV, which is ascribed to the photoemission from O 2s.[34] In comparison to the undoped NCD:H film, the C-related peaks (i.e., peaks i-iii) in the valence band spectrum of undoped NCD:O film are shifted toward higher binding energies. This shift can be attributed to the surface dipoles increasing the work function, which is consistent with the shift observed for C 1s core-level spectra in the undoped NCD:O film.[22,34] In addition, the photoemission peak due to O 2s (peak iv) is higher in intensity for the undoped NCD:O film compared to the undoped NCD:H film. This difference is in agreement with the higher O 1s/C 1s atomic concentration ratio in undoped NCD:O film.[22] Interestingly, for B-NCD:H and B-NCD:O films (Figure 4b), there is hardly any shift observed in the valence band binding energies. This could be due to the rather high boron doping in our film (boron concentration ~3000 ppm, bulk concentration of boron ≈ 1.6×10^{21} cm^{-3}), which pins the Fermi level at the boron level near the valence band.[35] The O 2s photoemission peak in B-NCD:H is found to be slightly lower in intensity as compared to B-NCD:O, which is not significant as compared to the differences observed in undoped NCD films. However, the WCA measurements of B-NCD:H and B-NCD:O surfaces showed a clear difference in surface wettability indicating different surface termination. The valence band data of the P-NCD films is given in Figure 4c and clearly shows that the Fermi level pinning is less dominant as compared to the B-NCD films.

To conclude from the first part of the Results and Discussion, the difference in the valence band spectra of undoped NCD:H and undoped NCD:O films is in line with the difference in the related band bending profiles, due to a shift in the Fermi level. On the contrary, the valence band spectra of the B-NCD:H and B-NCD:O films were found to be very similar, which can be understood by pinning of the Fermi level at the surface.

Next, the samples were studied with TRMC. Figure 5a shows a TRMC trace obtained on the excitation of undoped NCD:H

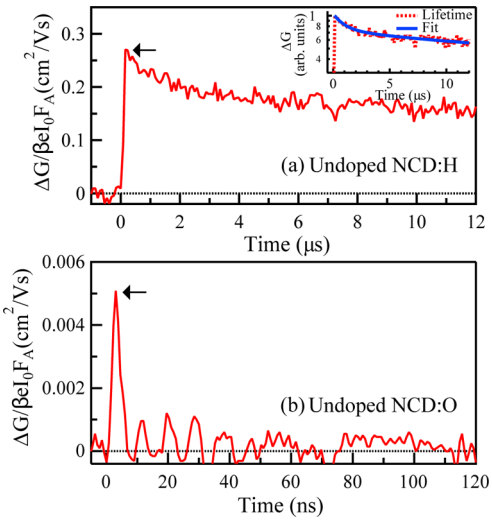

Figure 5. Photoconductance transient at 300 nm wavelength of the undoped NCD:H film plotted in two ways: (a) linear axes, showing the maximum value of $\Delta G/\beta e I_0 F_A$, indicated by the arrow and (inset) log-lin plot showing the charge carrier lifetime data (dotted line) and corresponding fit using a double exponential function (solid line). (b) Photoconductance transient of undoped NCD:O at 300 nm wavelength. The arrow indicates the maximum value of the photoconductance magnitude.

by a nanosecond laser pulse of 300 nm. From the trace two characteristic parameters can be extracted: the magnitude given by the maximum value of $\Delta G/\beta e I_0 F_A$ indicated by the arrow in Figure 5a, and second the decay time (inset in Figure 5a). According to eq 3, the value of $\Delta G/\beta e I_0 F_A$ corresponds to the product of the quantum yield of photoinduced charges (Φ) per absorbed photon and the sum of electron and hole mobilities ($\Sigma\mu$). Assuming a quantum yield of 1, a lower limit of ~0.27 $cm^2/(V\ s)$ for the sum mobility of the photogenerated charges is deduced. For undoped NCD:H mobility values up to 1 $cm^2/(V\ s)$ have been reported agreeing approximately with the values found in this work.[36] The inset of Figure 5a shows the lifetime (dotted line) of the photogenerated charge carriers and the resulting fit (solid line) using a double exponential function, yielding lifetimes of ~1 μs (τ_1) and ~10 μs (τ_2) (Table 1).

For undoped NCD:O (Figure 5b), the TRMC trace reaches a maximum value of only ~0.005 $cm^2/(V\ s)$, which is more than one order of magnitude smaller than the value of undoped NCD:H (Table 1). The trace resembles the shape of the laser pulse, indicating the lifetime of the photoinduced charges is less than a few nanoseconds, i.e., much shorter than that of undoped NCD:H. To estimate the charge carrier lifetime, the obtained transient is deconvoluted assuming a first-order decay (τ) and a mobility value of ~0.27 $cm^2/(V\ s)$ yielding a τ of ~100 ps.[24]

To study the influence of the charge carrier density on the photoconductance properties of undoped NCD:H, we performed TRMC experiments at various incident intensities

dx.doi.org/10.1021/am501907q | ACS Appl. Mater. Interfaces 2014, 6, 11368−11375

Table 1. Summary of the $\Phi\Sigma\mu$ and Lifetime Values for the Hydrogen- and Oxygen-Terminated Undoped, Boron-Doped, and Phosphorus-Doped NCD Films

	hydrogen-terminated			oxygen-terminated		
NCD film type	$\Phi\Sigma\mu$(cm^2/(V s)	lifetime		$\Phi\Sigma\mu$ (cm^2/(V s)	lifetime	
undoped NCD	~0.27	~1 μs (τ_1)	~10 μs (τ_2)	~0.005	~100 ps (τ)	
B-NCD	~0.040	~120 ns (τ_1)	~1.91 μs (τ_2)	~0.057	~108 ns (τ_1)	~1.78 μs (τ_2)
P-NCD	~0.0023	[a]		[a]	[a]	

[a]The signal-to-noise ratio of the TRMC signal was found to be too low to determine this value.

and wavelengths. Figure 6 (white section, top) shows the maximum values of the photoconductance expressed in $\Phi\Sigma\mu$ as

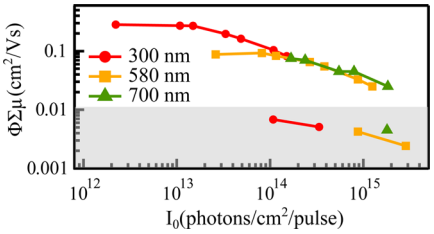

Figure 6. Photoconductance magnitude ($\Phi\Sigma\mu$) values as a function of intensity (I_0) for undoped NCD:H (white section, top) and undoped NCD:O (gray section, bottom) at different excitation wavelengths.

a function of the laser pulse intensity (I_0) at three different sub-bandgap wavelengths, i.e., 300, 580, and 700 nm. At $I_0 > 2 \times 10^{13}$ photons/cm^2, the value of $\Phi\Sigma\mu$ decreases with increasing intensity. This could be due to second-order recombination reducing the number of photoinduced mobile charges or due to charge carrier scattering resulting in a lowering of the mobility.[37] Interestingly, the dependence of the $\Phi\Sigma\mu$ values on I_0 is the same for all measured wavelengths. These results suggest that for undoped NCD:H the charge carrier generation and recombination kinetics are identical for all three photon energies.

Figure 6 (gray section, bottom) includes the maximum values of $\Phi\Sigma\mu$ for undoped NCD:O as a function of I_0 at the same three wavelengths. Only at intensities above 1×10^{14} photons/cm^2, a small photoconductance signal could be observed. For intensities less than 1×10^{14} photons/cm^2 the signal-to-noise ratio was too small to be resolved.

Because an electronic transition from the valence band to the conduction band of diamond requires an energy of ≥5.47 eV (~226 nm) all photon energies used in this work result in an electronic transition to or from an intrabandgap state; most likely an electron from the valence band to an empty π^* state. The differences observed in the TRMC results obtained for undoped NCD:H and undoped NCD:O can be rationalized by a change in the band bending diagram at the interface with air, because of the differences in surface termination. It has been reported previously that the electric dipoles caused by hydrogen atoms at the surface of diamond, lead to a reduction of the surface Fermi level (toward a decreased work function). This results in an upward band bending diagram in the presence of a water film at the diamond/air interface, facilitating the dissociation of an electron–hole pair formed on photoexcitation.[38−40] We postulate that upon sub-bandgap excitation of undoped NCD:H electrons are trapped in empty π^* states leaving behind mobile holes in the valence band (Figure 7a), which are drifted toward the surface. This suggests that the obtained mobility value of ~0.27 cm^2/(V s) from the

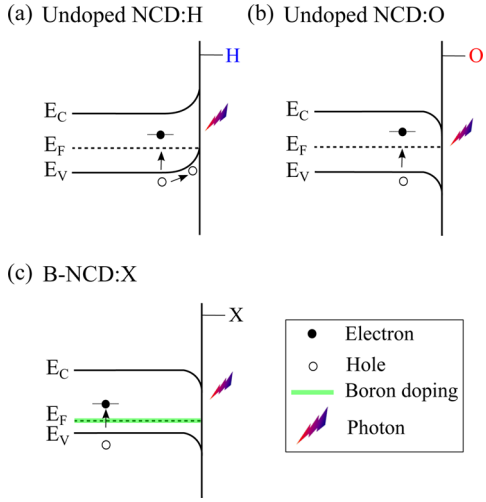

Figure 7. Qualitative band bending profiles for (a) undoped NCD:H, (b) undoped NCD:O and (c) B-NCD:X (X implies H or O). The arrows indicate the formation of electron–hole pair on photo-excitation. E_F, E_C, and E_V are the position of Fermi level, conduction band minimum and valence band maximum, respectively. The bandgap states between E_V and E_F act as hole traps, whereas bandgap states between E_F and E_C act as electron traps. The legend is given in the box on the bottom right side of the figure.

TRMC measurements is due to mobile holes, comparable to the hole mobility reported for both boron-doped and undoped hydrogenated NCD films.[8,21,36] The fact that the generation yield is independent of the three, largely varying wavelengths suggests that photoexcited electrons are trapped in common empty π^* states. In the case of undoped NCD:O, oxygen termination results in a downward band bending diagram due to the opposite electric dipole moment of oxygen as compared to hydrogen termination (Figure 7b).[40,41] Photoexcited electrons residing in π^* states are immobile, while the corresponding holes remain in the bulk of the grains of the NCD. Hence, fast second-order electron–hole recombination can take place explaining the rapid TRMC decay of ~100 ps. The band-bending diagram presented here to explain the TRMC results agrees well with the XPS valence band measurements on undoped NCD:H and undoped NCD:O (Figure 4a) discussed above, which show a shift in the surface Fermi levels.

To study the effect of doping on the optoelectronic properties of NCD, we performed TRMC measurements on boron (B-NCD) and phosphorus (P-NCD) doped films. Figure 8a shows the TRMC traces of hydrogen (B-NCD:H) and oxygen (B-NCD:O) terminated NCD, which interestingly are found to be similar. If Φ is assumed to be 1, the lower limit of the mobility is ~0.05 cm^2/(V s). Note that although a high boron concentration is used (boron concentration ~3000 ppm, bulk concentration of boron 1.6×10^{21} cm^{-3}) the majority of

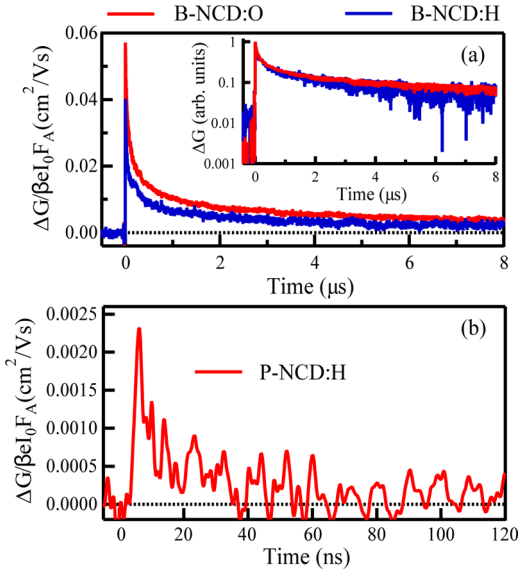

Figure 8. Photoconductance transients of (a) B-NCD and (b) P-NCD at 300 nm wavelength. Note the different time scales. The inset in a shows the charge carrier lifetime data for the B-NCD film.

dopants are not ionized. According to Baker et al., the high dopant concentration in crystalline diamond leads to Fermi level pinning near the valence band edge (Figure 7c).[35] Hence, it is expected that the surface dipole moments of the terminal groups do not affect the Fermi level. Thus, for boron-doped, hydrogen- or oxygen-terminated NCD, the band diagrams are equal, which explains the similar TRMC traces. In ambient conditions, a thin depletion layer is expected with a downward band bending, as shown in Figure 7c.[42] We suggest that on photoexcitation electrons are promoted to an empty π^* state. From there, the electrons could occupy a nonionized boron dopant, leaving a relatively long-lived mobile hole in the valence band (Table 1 for B-NCD lifetime values). This interpretation is in accordance with electrical conductivity measurements on highly doped, single-crystalline diamond films.[35] The present measurements demonstrate that also for NCD films doping leads to Fermi level pinning. Moreover, this model is in line with our interpretation of the XPS valence band measurements for B-NCD:H and B-NCD:O (Figure 4b) discussed above.

Figure 8b shows a TRMC trace of a P-NCD:H film, which reaches a maximum value of ~0.0023 $cm^2/(V\ s)$ and decays within a few nanoseconds. For P-NCD:O no detectable TRMC signal could be collected (data not shown). Clearly, the type of doping hugely affects the yield and lifetime of photogenerated charges. Phosphorus doping leads to a shift of the Fermi level toward the conduction band minimum.[43] There is not much literature on P-NCD films,[31,44] and to the best of our knowledge, it is not exactly known to what extent phosphorus doping leads to mobile electrons. Therefore, the position of the Fermi level is not clear, disabling picturing a band diagram. However, we suggest that optical excitation leads to population of an empty π^* state. In contrast to boron doping, electrons cannot be captured and will recombine rapidly, explaining the very short lifetimes observed in the TRMC traces.

4. CONCLUSION

The contactless TRMC technique along with the XPS has been used to study the effect of hydrogen and oxygen termination on the surface Fermi levels and the photoconductive properties of undoped and doped NCD films. The photoconductance signal and the charge carrier lifetimes are significantly affected by the type of surface termination on the undoped NCD films, whereas no surface termination effect was observed for boron-doped films. These results are explained on the basis of the differences in the band bending diagrams at the diamond surfaces. The photoconductance results from the TRMC technique provide a direct quantification of the charge carrier mobility and its decay dynamics without problems related to electrode contact issues. Furthermore, the charge transport study presented here provides valuable information to investigate the effect of surface functionalization on NCD films for potential surface-based (opto)electronic sensor applications and the charge transfer between diamond-organic systems for solar cell applications.[45]

AUTHOR INFORMATION

Corresponding Authors

*E-mail: t.j.savenije@tudelft.nl.
*E-mail: l.c.p.m.desmet@tudelft.nl.

Author Contributions

#Authors V.S. and D.H.K.M. contributed equally to this work.

Notes

The authors declare no competing financial interest.

ACKNOWLEDGMENTS

The authors thank Milos Nesládek (Hasselt University) for insightful discussions. The contribution of D.H.K.M. is part of the Dutch Polymer Institute (DPI, project #681) research program. This work was supported by the Delft University of Technology, the Hasselt University, the Research Program G.0555.10N of the Research Foundation-Flanders (FWO), the European Union (FP7) through the programs RODIN, MOLESOL, DIAMANT, DIADEMS, the Marie Curie ITN "MATCON" (PITN-GA-2009-238201), and the Marie Curie "STRENGTHNANO" (PIEF-GA-2011-300802).

REFERENCES

(1) Sussmann, R. S. *CVD Diamond for Electronic Devices and Sensors*; Wiley Publications: West Sussex, U.K., 2009.
(2) Nebel, C. E.; Shin, D.; Rezek, B.; Tokuda, N.; Uetsuka, H.; Watanabe, H. Diamond and Biology. *J. R. Soc., Interface.* **2007**, *4*, 439−461.
(3) Hubbard, H. M. Photovoltaics Today and Tomorrow. *Science* **1989**, *244*, 297−304.
(4) Lim, C. H. Y. X.; Zhong, Y. L.; Janssens, S.; Nesladek, M.; Loh, K. P. Oxygen-Terminated Nanocrystalline Diamond Film as an Efficient Anode in Photovoltaics. *Adv. Funct. Mater.* **2010**, *20*, 1313−1318.
(5) Williams, O. A. Nanocrystalline Diamond. *Diamond Relat. Mater.* **2011**, *20*, 621−640.
(6) Williams, O. A.; Nesladek, M.; Daenen, M.; Michaelson, S.; Hoffman, A.; Osawa, E.; Haenen, K.; Jackman, R. B. Growth, Electronic Properties and Applications of Nanodiamond. *Diamond Relat. Mater.* **2008**, *17*, 1080−1088.
(7) Achatz, P.; Garrido, J. A.; Stutzmann, M.; Williams, O. A.; Gruen, D. M.; Kromka, A.; Steinmuller, D. Optical Properties of Nanocrystalline Diamond Thin Films. *Appl. Phys. Lett.* **2006**, *88*, 1019081−1019083.
(8) Gajewski, W.; Achatz, P.; Williams, O. A.; Haenen, K.; Bustarret, E.; Stutzmann, M.; Garrido, J. A. Electronic and Optical Properties of Boron-Doped Nanocrystalline Diamond Films. *Phys. Rev. B* **2009**, *79*, 0452061−04520614.

(9) Nesladek, M.; Meykens, K.; Stals, L. M.; Vanecek, M.; Rosa, J. Origin of Characteristic Subgap Optical Absorption in CVD Diamond Films. *Phys. Rev. B* **1996**, *54*, 5552−5561.
(10) Remes, Z.; Kromka, A.; Potmesil, J.; Vanecek, M. Photocurrent Study of Electronic Defects in Nanocrystalline Diamond. *Diamond Relat. Mater.* **2008**, *17*, 1311−1315.
(11) Nebel, C. E.; Waltenspiel, A.; Stutzmann, M.; Paul, M.; Schafer, L. Persistent Photocurrents in CVD Diamond. *Diamond Relat. Mater.* **2000**, *9*, 404−407.
(12) Alvarez, J.; Kleider, J. P.; Bergonzo, P.; Tromson, D.; Snidero, E.; Mer, C. Study of Deep Defects in Polycrystalline CVD Diamond from Thermally Stimulated Current and Below-Gap Photocurrent Experiments. *Diamond Relat. Mater.* **2003**, *12*, 546−549.
(13) Kravets, R.; Ogorodniks, V.; Poruba, A.; Moravec, P.; Nesladek, M.; Rosa, J.; Vanecek, M. Fourier-Transform Photocurrent Spectroscopy of Defects in CVD Diamond Layers. *Phys. Status Solidi A* **2002**, *193*, 502−507.
(14) Nemec, P.; Preclikova, J.; Kromka, A.; Rezek, B.; Trojanek, F.; Maly, P. Ultrafast Dynamics of Photoexcited Charge Carriers in Nanocrystalline Diamond. *Appl. Phys. Lett.* **2008**, *93*, 0831021−0831023.
(15) Preclikova, J.; Trojanek, F.; Kromka, A.; Rezek, B.; Dzurnak, B.; Maly, P. Ultrafast Photoluminescence of Nanocrystalline Diamond Films. *Phys. Status Solidi A* **2008**, *205*, 2154−2157.
(16) Dzurnak, B.; Trojanek, F.; Preclikova, J.; Kromka, A.; Rezek, B.; Maly, P. Subgap Photoluminescence Spectroscopy of Nanocrystalline Diamond Films. *Diamond Relat. Mater.* **2009**, *18*, 776−778.
(17) Dzurnak, B.; Trojanek, F.; Preclikova, J.; Kromka, A.; Rezek, B.; Maly, P. Ultrafast Photoluminescence Spectroscopy of H- and O-Terminated Nanocrystalline Diamond Films. *Diamond Relat. Mater.* **2011**, *20*, 1155−1159.
(18) Kawarada, H.; Ruslinda, A. R. Diamond Electrolyte Solution Gate Fets for DNA and Protein Sensors Using DNA/RNA Aptamers. *Phys. Status Solidi A* **2011**, *208*, 2005−2016.
(19) Janssens, S. D.; Drijkoningen, S.; Saitner, M.; Boyen, H. G.; Wagner, P.; Larsson, K.; Haenen, K. Evidence for Phase Separation of Ethanol-Water Mixtures at the Hydrogen Terminated Nanocrystalline Diamond Surface. *J. Chem. Phys.* **2012**, *137*, 0447021−0447026.
(20) Williams, O. A.; Douheret, O.; Daenen, M.; Haenen, K.; Osawa, E.; Takahashi, M. Enhanced Diamond Nucleation on Monodispersed Nanocrystalline Diamond. *Chem. Phys. Lett.* **2007**, *445*, 255−258.
(21) Janssens, S. D.; Pobedinskas, P.; Vacik, J.; Petrakova, V.; Ruttens, B.; D'Haen, J.; Nesladek, M.; Haenen, K.; Wagner, P. Separation of Intra- and Intergranular Magnetotransport Properties in Nanocrystalline Diamond Films on the Metallic Side of the Metal-Insulator Transition. *New J. Phys.* **2011**, *13*, 0830081−08300818.
(22) Seshan, V.; Ullien, D.; Castellanos-Gomez, A.; Sachdeva, S.; Murthy, D. H. K.; Savenije, T. J.; Ahmad, H. A.; Nunney, T. S.; Janssens, S. D.; Haenen, K.; Nesladek, M.; van der Zant, H. S. J.; Sudhölter, E. J. R.; de Smet, L. C. P. M. Hydrogen Termination of CVD Diamond Films by High-Temperature Annealing at Atmospheric Pressure. *J. Chem. Phys.* **2013**, *138*, 2347071−2347076.
(23) Murthy, D. H. K.; Xu, T.; Chen, W. H.; Houtepen, A. J.; Savenije, T. J.; Siebbeles, L. D. A.; Nys, J. P.; Krzeminski, C.; Grandidier, B.; Stievenard, D.; Pareige, P.; Jomard, F.; Patriarche, G.; Lebedev, O. I. Efficient Photogeneration of Charge Carriers in Silicon Nanowires with a Radial Doping Gradient. *Nanotechnology* **2011**, *22*, 3157101−3157106.
(24) Savenije, T. J.; van Veenendaal, P.; de Haas, M. P.; Warman, J. M.; Schropp, R. E. I. Spatially Resolved Photoconductive Properties of Profiled Polycrystalline Silicon Thin Films. *J. Appl. Phys.* **2002**, *91*, 5671−5676.
(25) Savenije, T. J.; Ferguson, A. J.; Kopidakis, N. Rumbles, G. Revealing the Dynamics of Charge Carriers in Polymer: Fullerene Blends Using Photoinduced Time-Resolved Microwave Conductivity. *J. Phys. Chem. C* **2013**, *117*, 24085−24103.
(26) Geisler, M.; Hugel, T. Aging of Hydrogenated and Oxidized Diamond. *Adv. Mater.* **2010**, *22*, 398−402.
(27) Sun, Z.; Shi, J. R.; Tay, B. K.; Lau, S. P. UV Raman Characteristics of Nanocrystalline Diamond Films with Different Grain Size. *Diamond Relat. Mater.* **2000**, *9*, 1979−1983.
(28) Gonon, P.; Gheeraert, E.; Deneuville, A.; Fontaine, F.; Abello, L.; Lucazeau, G. Characterization of Heavily B-Doped Polycrystalline Diamond Films Using Raman Spectroscopy and Electron Spin Resonance. *J. Appl. Phys.* **1995**, *78*, 7059−7062.
(29) Michaelson, S.; Ternyak, O.; Hoffman, A.; Lifshitz, Y. Hydrogen Incorporation Processes in Nanodiamond Films Studied by Isotopic Induced Modifications of Raman Spectra. *Appl. Phys. Lett.* **2006**, *89*, 1319181−1319183.
(30) Ferrari, A. C.; Robertson, J. Interpretation of Raman Spectra of Disordered and Amorphous Carbon. *Phys. Rev. B* **2000**, *61*, 14095−14107.
(31) Janssen, W.; Turner, S.; Sakr, G.; Jomard, F.; Barjon, J.; Degutis, G.; Lu, Y. G.; D'Haen, J.; Hardy, A.; Van Bael, M.; Verbeeck, J.; Van Tendeloo, G.; Haenen, K. Substitutional Phosphorus Incorporation in Nanocrystalline CVD Diamond Thin Films. *Phys. Status Solidi RRL* **2014**, DOI: 10.1002/pssr.201409235.
(32) Souza, F. A.; Azevedo, A. F.; Giles, C.; Saito, E.; Baldan, M. R.; Ferreira, N. G. The Effect of Boron Doping Level on the Morphology and Structure of Ultra/Nanocrystalline Diamond Films. *Chem. Vap. Deposition* **2012**, *18*, 159−165.
(33) Bernard, M.; Deneuville, A.; Muret, P. Non-Destructive Determination of the Boron Concentration of Heavily Doped Metallic Diamond Thin Films from Raman Spectroscopy. *Diamond Relat. Mater.* **2004**, *13*, 282−286.
(34) Liu, F. B.; Wang, J. D.; Liu, B.; Li, X. M.; Chen, D. R. Effect of Electronic Structures on Electrochemical Behaviors of Surface-Terminated Boron-Doped Diamond Film Electrodes. *Diamond Relat. Mater.* **2007**, *16*, 454−460.
(35) Baker, S. M.; Rossman, G. R.; Baldeschwieler, J. D. Observation of Surface-Charge Screening and Fermi-Level Pinning on a Synthetic, Boron-Doped Diamond. *J. Appl. Phys.* **1993**, *74*, 4015−4019.
(36) Hubik, P.; Mares, J. J.; Kozak, H.; Kromka, A.; Rezek, B.; Kristofik, J.; Kindl, D. Transport Properties of Hydrogen-Terminated Nanocrystalline Diamond Films. *Diamond Relat. Mater.* **2012**, *24*, 63−68.
(37) Rossi, M. C.; Spaziani, F.; Salvatori, S.; Conte, G. Electronic Properties of Hydrogen and Oxygen Terminated Surfaces of Polycrystalline Diamond Films. *Phys. Status Solidi A* **2003**, *199*, 71−76.
(38) Maier, F.; Riedel, M.; Mantel, B.; Ristein, J.; Ley, L. Origin of Surface Conductivity in Diamond. *Phys. Rev. Lett.* **2000**, *85*, 3472−3475.
(39) Nebel, C. E.; Ertl, F.; Sauerer, C.; Stutzmann, M.; Graeff, C. F. O.; Bergonzo, R.; Williams, O. A.; Jackman, R. B. Low Temperature Properties of the P-Type Surface Conductivity of Diamond. *Diamond Relat. Mater.* **2002**, *11*, 351−354.
(40) Petrakova, V.; Taylor, A.; Kratochvilova, I.; Fendrych, F.; Vacik, J.; Kucka, J.; Stursa, J.; Cigler, P.; Ledvina, M.; Fiserova, A.; Kneppo, P.; Nesladek, M. Luminescence of Nanodiamond Driven by Atomic Functionalization: Towards Novel Detection Principles. *Adv. Funct. Mater.* **2012**, *22*, 812−819.
(41) Speranza, G.; Torrengo, S.; Filippi, M.; Minati, L.; Vittone, E.; Pasquarelli, A.; Dipalo, M.; Kohn, E. In Situ Thermal Treatment of UV-Oxidized Diamond Hydrogenated Surface. *Surf. Sci.* **2010**, *604*, 753−761.
(42) Diederich, L.; Kuttel, O.; Aebi, P.; Schlapbach, L. Electron Affinity and Work Function of Differently Oriented and Doped Diamond Surfaces Determined by Photoelectron Spectroscopy. *Surf. Sci.* **1998**, *418*, 219−239.
(43) Remes, Z.; Kalish, R.; Uzan-Saguy, C.; Baskin, E.; Nesladek, M.; Koizumi, S. Photo-Hall Measurements on Phosphorus-Doped N-Type CVD Diamond at Low Temperatures. *Phys. Status Solidi A* **2003**, *199*, 82−86.
(44) Hu, X. J.; Ye, J. S.; Hu, H.; Chen, X. H.; Shen, Y. G. Phosphorus Ion Implantation and Annealing Induced N-Type Conductivity and Microstructure Evolution in Ultrananocrystalline Diamond Films. *Appl. Phys. Lett.* **2011**, *99*, 1319021−1319023.

(45) Rezek, B.; Cermak, J.; Kromka, A.; Ledinsky, M.; Kocka, J. Photovoltage Effects in Polypyrrole-Diamond Nanosystem. *Diamond Relat. Mater.* **2009**, *18*, 249−252.